Food Chemistry 459 (2024) 140303

Contents lists available at ScienceDirect

Food Chemistry

journal homepage: www.elsevier.com/locate/foodchem

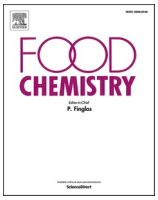

A synergistic solution for fighting fraudulent practices in squid using light stable isotope ratios and lanthanide tracers

Maria Olga Varrà [a], Lenka Husáková [b,*], Paola Iacumin [c], Martina Piroutková [b], Mattia Rossi [c], Jan Patočka [b], Sergio Ghidini [d], Emanuela Zanardi [a,*]

[a] Department of Food and Drug, University of Parma, 43126 Parma, Italy
[b] Department of Analytical Chemistry, Faculty of Chemical Technology, University of Pardubice, Studentska 573 HB/D, Pardubice, CZ-532 10, Czech Republic
[c] Department of Chemistry, Life Sciences and Environmental Sustainability, University of Parma, 43124 Parma, Italy
[d] Department of Veterinary Medicine and Animal Sciences Milan University, 26900 Lodi, Italy

ARTICLE INFO

Keywords:
Rare earth elements
Light stable isotopes, country-of-origin labelling
Traceability
Machine learning

ABSTRACT

To identify a novel optimized strategy for preventing fraudulent substitutions of squid species and origins, forty European squids (*Loligo vulgaris*) and forty flying squids (*Todarodes sagittatus*) from the Mediterranean Sea and Atlantic Ocean were analyzed for $\delta^{13}C$, $\delta^{15}N$, La, Ce, Pr, Nd, Sm, Eu, Gd, Tb, Dy, Ho, Er, Yb, and Lu using isotope ratio mass spectrometry and inductively coupled plasma-mass spectrometry. While $\delta^{13}C$ and $\delta^{15}N$ variations were mainly species-related, they alone could not reliably distinguish samples. To address this issue, decision rules were developed using Classification and Regression Tree analysis. Threshold values for $\delta^{13}C$ (−19.91‰), $\delta^{15}N$ (14.87‰), and Pr (0.49 μg kg^{-1}) enabled successful discrimination among Mediterranean European squids, Atlantic European squids, Mediterranean flying squids, and Atlantic flying squids, achieving over 90% accuracy, 81% precision, 80% sensitivity, and 93% specificity. This method holds promise for enhancing traceability and safety in the seafood industry, ensuring product integrity and consumer trust.

1. Introduction

Traceability within the fish industry is essential for combating fraud, allowing free choices of consumers, and assuring safety. Fish and seafood pose more intricate traceability challenges compared to other foods due to a variety of factors, which include the wide range of species and production methods, international trade, their perishable nature necessitating rapid handling, and the multiple processing, packaging, and transportation stages they typically undergo (Costa Leal et al., 2015; Varrà, Zanardi, et al., 2023). All these aspects increase the risk of unintentional or fraudulent product substitution, which can particularly impact valuable fishery products. In response to these challenges, EC Regulation 178/2002 and EU Regulation 1379/2013 collaboratively established a comprehensive framework for traceability at all stages of production, processing, and distribution within the fish and seafood industry. This framework also mandates the provision of critical information such as commercial and scientific names of the species, production methods, and the origin of fisheries on product labels (European Commission, 2002; European Union, 2013).

European squids and flying squids are two squid species widely distributed throughout the Mediterranean Sea and the North-Eastern Atlantic Ocean, representing significant food resources for the European population. The market value of these two species varies as a function of their distinct geographical fishing regions. Furthermore, European squid is typically priced higher than flying squid, primarily because of its superior taste and textural qualities, which can be attributed to differences in their biochemical composition, such as higher amino acid and lower glycogen contents in European squid compared to flying squid (Rosa et al., 2005). In addition to economic considerations, squids may exhibit distinct food safety profiles. Contamination by organic pollutants, toxins, parasites, and heavy metals may indeed vary significantly depending on both the place of origin and the biological species. For instance, flying squids have more frequently been associated with higher concentrations of heavy metals

Abbreviations: MES, Mediterranean European squids; AES, Atlantic European squids; MFS, Mediterranean flying squids; AES, Atlantic flying squids; ICP-MS, inductively coupled plasma-mass spectrometry; IRMS, isotope ratio mass spectrometry; ROC, Receiver Operating Characteristic; AUROC, Area Under the Receiver Operating Characteristic.

* Corresponding author.
E-mail address: emanuela.zanardi@unipr.it (E. Zanardi).

https://doi.org/10.1016/j.foodchem.2024.140303
Received 28 March 2024; Received in revised form 21 June 2024; Accepted 30 June 2024
Available online 10 July 2024

due to different physiology and feeding habits (Miedico et al., 2015; Varrà, Husáková, et al., 2023). This is particularly true for Hg concentrations, which were reported to be ten times higher in flying squid compared to European squid (median values: 0.31 mg kg^{-1} vs. 0.069 mg kg^{-1}). The difference is even more pronounced for Cd contamination, with flying squid showing concentrations in soft tissues up to two orders of magnitude higher than those in European squid (median values: 0.33 mg kg^{-1} vs. 0.0050 mg kg^{-1}) (Varrà, Husáková, et al., 2023). This disparity could potentially be attributed to the presence of heterolysosomes and heterophagosomes, structures found only in flying squid, which are responsible for the storage, detoxification, and mobilization of Cd and other metallic contaminants in their tissues Varrà, Husáková, et al., 2023).

Given that mislabeling of cephalopod species was reported to occur in up to 44% of cases, testing squids for their authenticity in terms of both biological species but also geographical origin is essential to maintain the integrity of the entire supply chain and ensure consumer safety (Guardone et al., 2017). Typically, the external and internal characteristics of squids are analyzed morphologically and morphometrically to determine their authenticity. Nevertheless, anatomical traits do not vary according to the geographical origin and cannot be used to differentiate squid species when they are sold as prepared or processed products, as specific morphological features may be absent (Khaksar et al., 2015). DNA-based analytical methods can be used to identify squid species with high sensitivity, but they are not accurate enough to determine the geographical origin of populations that are geographically close populations due to gene flow between them (Costa Leal et al., 2015). Chemical methods based on the profiling of organic molecules (e.g., fatty acids, amino acids, sugars, metabolites), on the contrary, have demonstrated great potential for ascertaining the geographical provenance, but they are less useful for species testing and complicated by several confounding pre-catch (seasonality, fish size, reproductive status, migration) as well as post-catch variables (storage conditions and processing) (Danezis, Tsagkaris, Camin, et al., 2016).

Inorganic chemical profiles, encompassing stable isotope ratios of light elements (H, C, N, S) and multi-elemental concentrations, have emerged as powerful tools for multipurpose authentication of fish and seafood products, exhibiting high stability over time with minimal impact from food processing (Katerinopoulou et al., 2020; Martino et al., 2019; Martino et al., 2022).

Isotope ratios of carbon ($^{13}C/^{12}C$, $\delta^{13}C$) and nitrogen ($^{15}N/^{14}N$, $\delta^{15}N$) have historically served as precise and sensitive tools for the verification of biological species, farming practices, production methods, and geographical origins (Danezis et al., 2016a; del Rio-Lavín et al., 2022; Tulli et al., 2020; Varrà, Zanardi, et al., 2023; Xu et al., 2022). More specifically, $\delta^{13}C$ values are modulated by factors such as solar irradiance, the prevalence of C3 and C4 carbon fixation pathways in aquatic plants, and the nutrient flux within aquatic environments, thus being useful as a direct marker of species and an indirect marker of geographical origin (Carrera & Gallardo, 2017). The $\delta^{15}N$ value reflects N fixation carried out by cyanobacteria and other microorganisms in the water column (Carrera & Gallardo, 2017), with higher $\delta\ ^{15}N$ values in fish typically linked to an elevation in trophic levels (Kim et al., 2015). This enrichment has been exploited as a good indicator of metabolic activity, stress levels, and dietary preferences of fish (Kim et al., 2015), as well as a valuable tool for species differentiation (Gong et al., 2018; Zhang et al., 2017).

On the other hand, compared to other naturally occurring trace elements, lanthanides have a stronger association with the geochemical characteristics of the soils where they naturally occur. In particular, the concentrations and distributions of lanthanides in marine environments are influenced by a combination of natural geogenic processes (such as volcanic activity, ice melting, hydrothermal vents, and groundwater flow) and human activities (such as oil- and coal-fired power plants, metallurgical and electronic industries, and incineration processes) (Patel et al., 2023; Piarulli et al., 2021). The lanthanide signature is therefore very site-specific and accurately reflects the source water from which the fish and seafood are caught. This trait makes them promising candidates for use as emerging tracers in investigations focused on determining the geographical origin of foods (Danezis et al., 2017; Danezis, Tsagkaris, Brusic, & Georgiou, 2016).

Recent research applications have primarily focused on the combined use of isotope ratios and trace-element profiles (excluding lanthanides) for assessing the origin, species, or production method of fish, but applications to cephalopods have been very scarce, being limited to octopus (Gong, Chen, & Chen, 2018; Martino et al., 2022). The integration of stable isotope ratios and lanthanides for the purpose of fish authentication has been explored in just one prior study (Varrà et al., 2019). While this study showed promising results, it was limited in scope as it examined only a restricted set of lanthanides.

The present study was driven by the hypothesis that the integration of complementary information derived from stable isotope ratios of carbon ($\delta^{13}C$) and nitrogen ($\delta^{15}N$), in conjunction with lanthanide profiles, could, for the first time, enable the accurate differentiation of squids based on their geographical origin (Mediterranean Sea vs. northeastern Atlantic Ocean) and biological species (*Loligo vulgaris* vs. *Todarodes sagittatus*). This innovative approach aims to bolster control measures for cephalopods, resulting in a comprehensive enhancement of traceability and safety standards for these products.

2. Materials and methods

2.1. Sample description and experimental design

A sample size of 80 specimens of two commercial squid species caught from two different geographic areas was provided by trusted suppliers. Of these, 40 were European squids (*Loligo vulgaris*, 14 ± 1 cm dorsal mantle length, 150–200 g weight) and 40 were flying squids (*Todarodes sagittatus*, 20 ± 2 cm dorsal mantle length, 200–250 g weight). For each species, 20 samples were collected from the central Mediterranean Sea (Northern Adriatic Sea, FAO fishing area 37.2.1) and 20 samples were collected from the North-Eastern Atlantic Ocean (North-Western coasts of Scotland and Ireland, FAO fishing areas 27.6 and 27.7).

To ensure a broad representation of the populations, three different batches per squid species and per geographical origin were included in the sample set. Within each batch, Mediterranean European squids (MES), Atlantic European squids (AES), Mediterranean flying squids (MFS), and Atlantic flying squids (AFS) of both sexes were included. These specimens were all caught during the autumn-winter fishing season using trawl nets. To account for potential temporal and spatial variability, they were fished at various times and by different fishing vessels from multiple locations within each region.

To minimize selection bias and enhance the representativeness of the sample groups, specimens designated for analysis were randomly selected from each batch and assigned a unique identifier.

2.2. Preparation of squid samples

Squids were transported on ice to the laboratory, where they were immediately frozen and stored at −21 ± 2 °C until preparation. After overnight defrosting at +4 °C ± 2 °C, each specimen was washed with deionized water, eviscerated, and its deskinned mantle was finely minced using a knife. Each sample (approx. 30 g of minced mantle) was frozen at −80 ± 2 °C for 24 h and afterwards subjected to freeze-drying for 24–36 h at 0.001–0.002 mbar pressure and − 55 °C using a LyoQuest Plus −55 freeze-drier (Telstar Co., Terrassa, Spain). The dried samples were finally ground to homogenous powder using ceramic mortars and pestles and stored in sealed bags at refrigerated temperature (+4 ± 2 °C).

2.3. Analysis of carbon and nitrogen isotopes via isotope ratio mass spectrometry (IRMS)

Freeze-dried powdered samples (0.2 mg) or reference materials (RMs) were weighted using an electronic microbalance (Sartorius M2P, Sartorius AG, Göttingen, Germany) and wrapped into 3.3 × 5.0 mm cylindric tin capsules. Isotopic analyses of C and N were conducted using an elemental CHN analyzer (Flash HT 2000, Thermo Fisher Scientific Inc., Bremen, Germany) coupled to a Delta V Advantage IRMS (Thermo Fisher Scientific Inc., Bremen, Germany). The results were expressed using the δ notation relative to the international standards Vienna Pee Dee Belemnite (V-PDB) for $\delta^{13}C$ and atmospheric Air (air-N_2) for $\delta^{15}N$ values using the following equation: $\delta^{13}C$ or $\delta^{15}N = 10^3$ x ((R_{sample}/R_{RM}) – 1), where R_{sample} and R_{RM} were the ratio of the heavy to the light isotope ($^{13}C/^{12}C$ or $^{15}N/^{14}N$) of the sample and RMs, respectively.

Urea (20.00% C and 46.65% N) was used as internal laboratory standard for calculating the percentages of C and N in the samples. The precision (expressed as percent relative standard deviation, RSD %) of the analysis of urea was ±3%. The δ values of the samples were measured versus a tank ultrapure CO_2 or N_2 gas. In order to monitor the accuracy and repeatability of the measurements and to calibrate the δ values, a calibration line with three international RMs with known isotope value was used. For $\delta^{15}N$ the IAEA N-1 (ammonium sulphate), IAEA N-2 (ammonium sulphate), USGS-32 (potassium nitrate) and, as sample for quality control, USGS-25 (ammonium sulphate) were analyzed. For $\delta^{13}C$ USGS-24 (graphite), NBS-22 (mineral oil), IAEA-CH-6 (sugar), and, as sample for quality control, IAEA-CH-6 (polyethylene) were analyzed. The precision of the measurements was 0.2‰ for both $\delta^{13}C$ and $\delta^{15}N$ values.

2.4. Analysis of lanthanides via inductively coupled plasma-mass spectrometry (ICP-MS)

The method used for analyzing samples for lanthanide quantification was adapted from a previously described and validated method (Varrà et al., 2021). A mixture of 1 mL of 30% (*v*/v) H_2O_2 and 4 mL of 16% (v/v) HNO_3 was added to 100 mg of either samples or certified reference materials (CRMs) in order to prepare the samples for analysis. The samples underwent digestion using a Speedwave™ MWS-3$^+$ microwave oven (Berghof, Eningen, Germany) equipped with a magnetron capable of delivering a maximum power of 1450 W. The temperature program included a first step at 180 °C for 5 min with a ramp, followed by hold times of 5 and 20 min, respectively. The second step was conducted at 220 °C with a ramp of 5 min and a hold for 20 min. Subsequently, a cooling phase down to 100 °C was achieved within 5 min, followed by a 5-min hold period. The resulting digested solutions were diluted with ultrapure water to obtain a final volume of 25 mL.

The quantification of the lanthanides was carried out using a quadrupole ICP-MS instrument Agilent 7900 (Agilent Technologies, Inc., Santa Clara, CA, USA) equipped with a fourth generation ORS^4 octopole collision/reaction cell to attenuate spectral overlaps. The samples and internal standard (ISTD) were introduced directly into the ICP-MS system using a low-pulsation, 10-roller peristaltic pump and an Agilent SPS 4 autosampler. The ICP-MS configuration involved the use of a standard sample introduction system, which included a MicroMist glass concentric nebulizer, a Peltier-cooled quartz spray chamber, and a quartz torch featuring a 2.5 mm ID injector. The interface was comprised of a nickel-plated copper sampling cone and a nickel skimmer cone. A 200 μg L^{-1} Rh internal standard solution was prepared from a 1 g L^{-1} stock solution (SCP Science, Montreal, Canada) and added on-line to all standards and samples using the standard ISTD mixing tee-connector to adjust for instrument instability, signal drifts, and non-spectral interferences. Information regarding the analytical parameters and operational settings used in the ICP-MS analysis is reported in Table S1 (Supplementary Material).

Five calibration standards were prepared to accurately quantify the target analytes, covering La, Ce, Pr, and Nd in the range of 0–10 μg L − 1, and Sm, Eu, Gd, Tb, Dy, Ho, Er, Yb, and Lu within the 0–2 μg L^{-1} range. Calibration solutions were prepared daily by proper dilution of a stock solution containing 50 mg L^{-1} of La, Ce, Pr, Nd and 10 mg L^{-1} of Tb, Ho, Yb, Sm, Eu, Gd, Er, Lu, and Dy which, in turn, was prepared from the commercial multi-element standard of the rare earth elements Astasol mix M008 (Analytika Ltd., Prague, Czech Republic). Following calibration, a coefficient of determination higher than 0.999 for all the analytes was obtained.

The sensitivity of the method was assessed by determining the method limits of detection (MLODs) for each element. This was done to ensure the reliability and meaningful interpretation of the analytical results. MLODs were computed as the concentrations of samples producing a signal-to-noise ratio of 3 times the standard deviation derived from 10 replicates of a blank sample. The MLODs for each element can be found in Table S2 of the Supplementary Material.

The overall accuracy of the measurements was evaluated by analyzing the following CRMs: CRM 12–2-01 Bovine Liver (pb-anal, Kosice, Slovakia); CRM 12–2-03 P-Alfalfa essential and toxic elements in Lucerne (pb-anal, Kosice, Slovakia); GBW 10052 Green Tea (Chinese Academy of Geological Sciences, Beijing, China); NCS ZC73015 Milk Powder (National Research Centre for Certified Reference Materials, NRCRM, Beijing, China). The percentage recovery values, comparing certified and measured values, along with intra-day and inter-day precision values (expressed as RSD%), consistently exceeded 86% and remained below 10% for all tested elements (refer to Supplementary Material, Table S3).

2.5. Data processing, statistics, and machine learning

Data from isotopic and lanthanide analysis were corrected for non-normal distribution and heteroscedasticity (assessed though the application of the Shapiro-Wilk's and the Levene's test at 95% confidence level, respectively) using a Box-Cox transformation. To express the data in a summary form, mean and 95% confidence interval (CI, lower and upper) values were calculated for all the analytes measured in each of the squid classes under investigation (i.e., MES, AES, MFS, and AFS) and reported on the original scale after the Box-Cox data were back-transformed using the inverse formulas.

The Analysis of Variance (ANOVA) was employed to transformed data to assess the statistical significance of differences of the measured isotopic and lanthanide values among the different squid groups (i.e., MES vs. AES vs. MFS vs. and AFS). The confidence level to identify statistically significant differences was set at 95% ($p \leq 0.05$).

The Box-Cox transformed data matrix was further standardized through *Z*-score normalization (scaling to a range of 0–1) to ensure comparability of isotopic and lanthanide data on a consistent scale. Subsequently, the Pearson's correlation analysis was applied to provide a more comprehensive exploration of the bivariate relationships among isotopes and lanthanides. In this analysis, strong positive or negative co-variations were pinpointed through correlation coefficients (r) ≥ 0.6 or ≤ -0.6, respectively, while the statistical significance of the co-variation was set at $p \leq 0.05$.

In order to visualize the distribution of the samples in a multivariate space, the *k*-means cluster analysis was applied, using the Euclidean distance metric to allocate points to individual clusters while setting the maximum number of iterations to 10. The optimal number of clusters, denoted as "*k*", was determined through the application of the Silhouette method and selected based on the highest average Silhouette width as *k* values ranged from 2 to 15. The Silhouette coefficients offer insight into how well each sample is placed within a cluster, i.e., how much a sample is far from the neighboring wrong cluster and close to its correct cluster. Specifically, Silhouette coefficients span the range from −1 to +1, where values close to −1 indicate a wrong placement, those close to 0 indicate an ambiguous placement, and those close to +1 indicate a correct placement (Rousseeuw, 1987).

In the last step, the non-transformed (raw) data matrix was subjected to classification techniques based on decision trees chosen from the machine learning toolkit. The employed algorithm was the Classification and Regression Tree (CART), used to formulate rules for the simultaneous classification of samples into one of the four target classes under consideration and to simultaneously extract the most significant variable for classification. This selection was motivated by its non-parametric nature, robustness toward outliers, high interpretability, and practical utility, all of which enhance result interpretation, communication, and overall applicability (Jiménez-Carvelo et al., 2019). Moreover, the CART algorithm is integrated into many open-access platforms and software, offering the advantage of being accessible and available to the widest possible range of users. The decision tree was constructed using the Gini Impurity Index which, measuring the probability of misclassifying a randomly selected sample based on the distribution of class labels within the dataset, select the most appropriate variables for data splitting within each node of the tree. To mitigate the risk of overfitting and excessive complexity of the tree, a maximum depth of five tree levels was established a priori. The criterion employed during the tree-building process to select the optimal final classification tree was the minimization of misclassification cost. The CART was run on 60 randomly selected squid specimens (i.e., 15 samples per group, 75% of the total number), which were used to train and build the classification model (training set). The remaining 20 samples (i.e., 5 samples per group, 25% of the total number) were set aside for the purpose of validating the trained model (test set). This process aimed to simulate a real-world scenario where the model is used to predict the class membership of new, previously unobserved samples.

The overall performances of the CART model were evaluated in both the training and validation phases by examining the percentages of true positives (TP), true negatives (TN), false positives (FP), and false negatives (FN) resulting from the classification. Additionally, percentages of key performance metrics were calculated, including accuracy ((TP + TN) / (TP + TN + FP + FN)), precision (TP / (TP + FP)), sensitivity (TP / (TP + FN)), and specificity (TN / (TN + FP)) (Fawcett, 2006). Finally, the trade-off between sensitivity and 1–specificity for both the training and test sets was assessed by generating the Receiver Operating Characteristic (ROC) curves for each of the squid classes under investigation. The Area Under the Receiver Operating Characteristic (AUROC) curves (which ranges from 0 to 1, where 0 indicates poor model performance and 1 represents perfect model performance) was calculated, and values >0.5 were deemed the threshold for defining the ability of the classification tree to effectively distinguish the class of interest from others (Fawcett, 2006).

Data analysis, including statistics and machine learning, was performed using OriginPro 2021 (v. 9.8.0.200, Origin Lab Corporation, USA) and Orange Data Mining© (v. 3.36.2, University of Ljubljana, https://orangedatamining.com/) software packages.

3. Results

3.1. Isotope ratios, lanthanide concentrations, and their correlations

Summary statistics for $\delta^{13}C$, $\delta^{15}N$, and the concentrations of the 13 lanthanides (including mean values and 95% CI ranges calculated after the reversion of the Box-Cox transformation, see *Section 2.5*), along with the results of the ANOVA test followed by Tukey's post-hoc analysis, are provided in Table 1. Significantly higher values of $\delta^{13}C$ and $\delta^{15}N$ were observed in MES (−18.47 and 15.03‰, respectively) in comparison to the other sample groups ($p \leq 0.05$). Conversely, the lowest $\delta^{13}C$ values were recorded in AFS (−20.23‰), while the lowest $\delta^{15}N$ values were found in both MFS (11.76‰) and AES (12.01‰) ($p \leq 0.05$). The C/N ratios was found to be lower in AFS, followed by MFS, EAS, and AFS, with values ranging from a minimum of 3.41 to a maximum of 4.24 (Table 1).

Regarding lanthanide concentrations, the overall sum of the 13 measured elements was found to range from a minimum of 12.7 μg kg^{-1} in AES to a maximum of 48.1 μg kg^{-1} in MFS, with AFS and MES samples showing intermediate concentrations (32.5–34.4 μg kg^{-1}).

Ce emerged as the most abundant element, with levels ranging from approximately 6.00 to 30.0 μg kg^{-1} in all samples. In contrast, Lu was found to be the least abundant one, with concentrations varying approximately from 0.02 to 0.11 μg kg^{-1} (Table 1). AES showed significantly higher concentrations of Pr and Nd and significantly lower concentrations of Ce, Sm, Gd, Dy, Ho, Er, Yb, and Lu ($p \leq 0.05$, Table 1). Ho was found to be the sole element that exhibited variation based on

Table 1
Mean values[#] and 95% lower (L) and upper (U) confidence limits[#] of the isotopes and lanthanides[*] in the analyzed squid samples.

	Flying squid						European squid					
	Atlantic			Mediterranean			Atlantic			Mediterranean		
	Mean	L	U	Mean	L	U	Mean	L	U	Mean	L	U
10^3 x $\delta^{13}C$	-20.23^{c}	−19.90	−20.56	-19.19^{b}	−18.89	−19.49	-19.38^{b}	−19.22	−19.44	-18.47^{a}	−18.30	−18.64
C %	47^{a}	43.3	49.7	45^{b}	44.0	45.9	43^{c}	42.3	46.6	45^{b}	45.3	47.1
10^3 x $\delta^{15}N$	13.25^{b}	12.73	13.75	11.76^{c}	11.01	12.46	12.01^{c}	11.6	12.39	15.03^{a}	14.71	15.33
N %	12^{b}	11.4	11.7	11^{c}	11.1	11.5	11^{c}	11.1	12.3	13^{a}	12.3	13.8
C/N	4.03^{a}	3.80	4.24	3.95^{ab}	3.96	4.00	3.82^{b}	3.83	3.79	3.45^{c}	3.68	3.41
La	3.71^{ab}	4.49	3.11	3.94^{a}	3.45	4.56	1.88^{c}	1.61	2.22	2.74^{b}	2.32	3.29
Ce	15.4^{ab}	8.9	26.68	26.23^{a}	19.19	35.85	8.13^{b}	5.9	11.18	20.85^{a}	14.7	29.56
Pr	1.86^{ab}	1.34	2.63	2.44^{a}	1.76	3.47	0.18^{c}	0.15	0.23	1.03^{b}	0.73	1.49
Nd	4.57^{ab}	3.33	6.44	6.95^{a}	5.09	9.75	0.51^{c}	0.42	0.61	2.81^{b}	1.98	4.12
Sm	1.59^{ab}	1.12	2.25	2.05^{a}	1.48	2.84	0.14^{c}	0.11	0.23	1.04^{b}	0.72	1.5
Eu	0.51^{bc}	0.38	0.7	0.64^{ab}	0.51	0.82	0.31^{c}	0.2	0.5	1.07^{a}	0.78	1.45
Gd	1.25^{ab}	0.89	1.74	1.57^{a}	1.17	2.12	0.22^{c}	0.16	0.25	0.74^{b}	0.51	1.09
Tb	0.57^{b}	0.45	0.73	0.58^{b}	0.45	0.77	0.77^{b}	0.51	1.24	2.16^{a}	1.49	3.22
Dy	1.29^{ab}	0.98	1.69	1.62^{a}	1.23	2.13	0.21^{c}	0.17	0.26	0.83^{b}	0.61	1.14
Ho	0.25^{a}	0.2	0.33	0.33^{a}	0.22	0.42	0.04^{c}	0.04	0.05	0.15^{b}	0.11	0.2
Er	0.75^{ab}	0.59	0.94	0.87^{a}	0.66	1.13	0.11^{c}	0.08	0.14	0.45^{b}	0.33	0.62
Yb	0.65^{ab}	0.5	0.83	0.71^{a}	0.55	0.92	0.13^{c}	0.08	0.13	0.43^{b}	0.33	0.56
Lu	0.11^{a}	0.09	0.14	0.12^{a}	0.10	0.15	0.02^{b}	0.02	0.04	0.08^{a}	0.06	0.11
ΣLan[$]	32.5^{b}	23.3	48.2	48.1^{a}	35.9	61.5	12.7^{c}	9.45	17.1	34.4^{b}	24.7	48.4

Significant differences among the four groups of samples reported in each raw (resulting from ANOVA followed by Tukey's post-hoc test, $p \leq 0.05$) are indicated by different superscript letters, ranging from "a" (representing the highest concentration) to "c" (indicating the lowest concentrations).

[#] Back-transformed data calculated after reversing the Box-Cox transformation (except for $\delta^{13}C$).

[*] Lanthanide concentrations are reported in μg kg^{-1}.

[$] Cumulative concentration of the 13 measured lanthanides (μg kg^{-1}).

biological species, with higher concentrations observed in both AFS and MFS when compared to AES and MES ($p \leq 0.05$).

The analysis of co-variation patterns among the variables, resulting from the application of Pearson's correlation analysis to the transformed and scaled data matrix, is graphically summarized in the correlation matrices reported Fig. 1. Significant correlations were mainly limited to the lanthanide elements, with no correlations identified among C and N isotopes except for AES ($r = -0.67$) (Fig. 1B). Globally, these correlation patterns were found to be consistent across all analyzed squid groups, regardless of their origin and biological species, but their strength varied depending on the specific sample group (Fig. 1 A-D). In particular, significant strong positive bivariate correlations ($r \geq 0.6$, $p \leq 0.05$) between Eu—Lu and significant strong negative bivariate correlations ($r \leq -0.6$, $p \leq 0.05$) between La—Ce, La—Dy, Pr—Dy, and Pr—Eu were identified in samples belonging to all the groups considered. AES samples, in addition, were identified as the group showing the highest number of covariation patterns among the analyzed elements (Fig. 1B).

3.2. Clustering of squid samples

The box plots reported in Fig. 2 summarize the distribution of $\delta^{15}N$ and $\delta^{13}C$ values in the analyzed squid samples. It is evident that the MFS groups exhibited the greatest variability in both $\delta^{15}N$ and $\delta^{13}C$ values compared to the other sample groups (Fig. 2A and Fig. 2B). Conversely, $\delta^{15}N$ values demonstrated a more uniform distribution among samples within the AES groups (Fig. 2A), whereas $\delta^{13}C$ values were more evenly spread among samples in the AFS groups (Fig. 2B).

A preliminary bidimensional representation illustrating the distribution of all 80 squid samples, based solely on their $\delta^{13}C$ and $\delta^{15}N$ values, is depicted in Fig. 3. The remarkably high degree of within-class heterogeneity of MFS samples emerged again, as they spanned a wider area within the bidimensional plot compared to the other groups. Upon closer examination of the $\delta^{13}C$ values, a separation between MES and AFS became evident, delineating two opposing and not overlapping sample groups. When focusing on samples collected from the Mediterranean Sea, European squid (MES) tended to separate from flying squid (MFS) primarily due to their higher $\delta^{15}N$ values. However, this differentiation was not observed among the two species collected from the

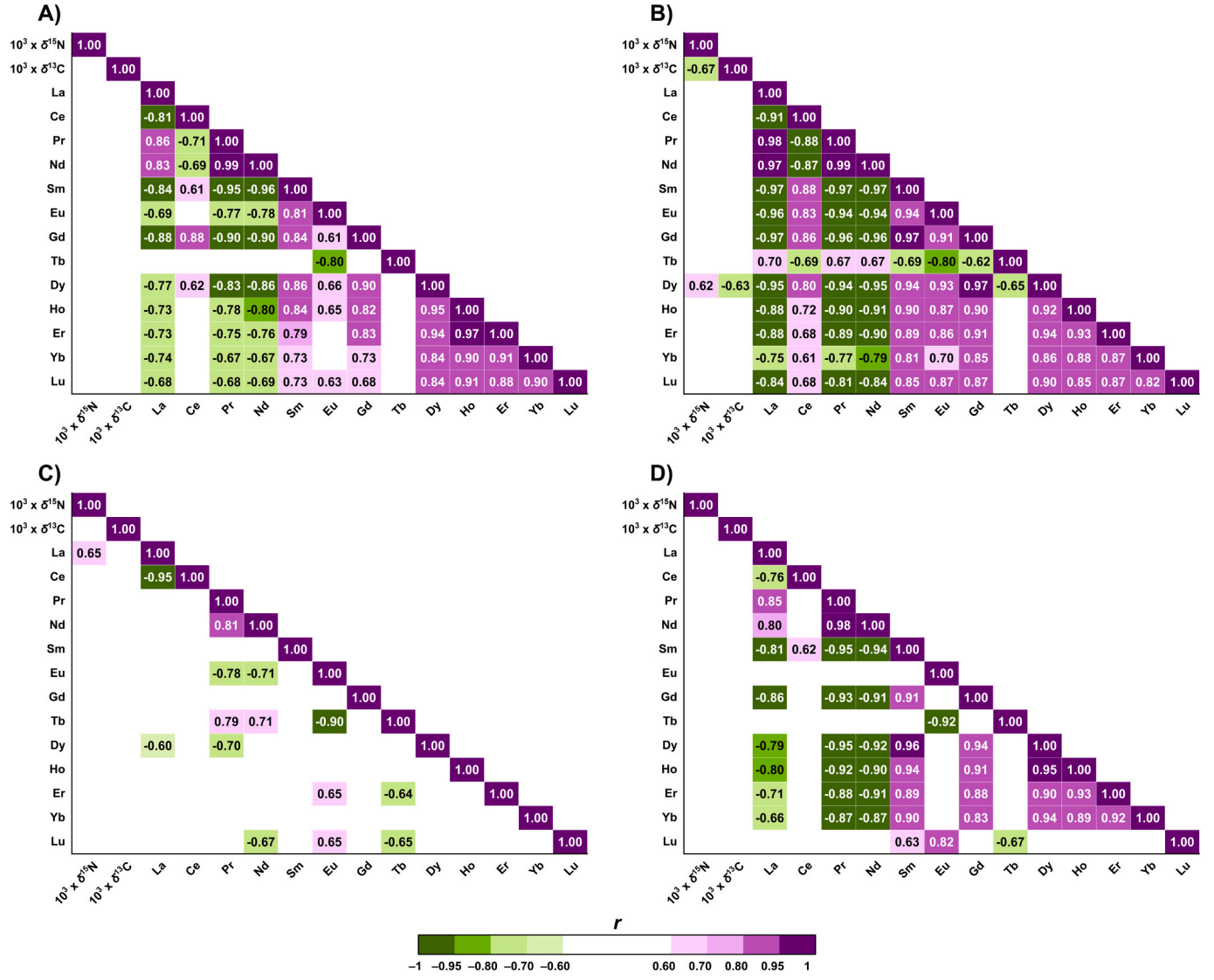

Fig. 1. Heat maps resulting from Pearson's pairwise correlation analysis of isotope ratios and lanthanides measured in Atlantic flying squid (**A**), Mediterranean flying squids (**B**), Atlantic European squids (**C**), and Mediterranean European squids (**D**). Only statistically significant correlations ($p \leq 0.05$) with $r > 0.6$ or $r \leq -0.6$ are displayed and color-coded from deep purple (positive correlations) to deep green (negative correlations). (For interpretation of the references to color in this figure legend, the reader is referred to the web version of this article.)

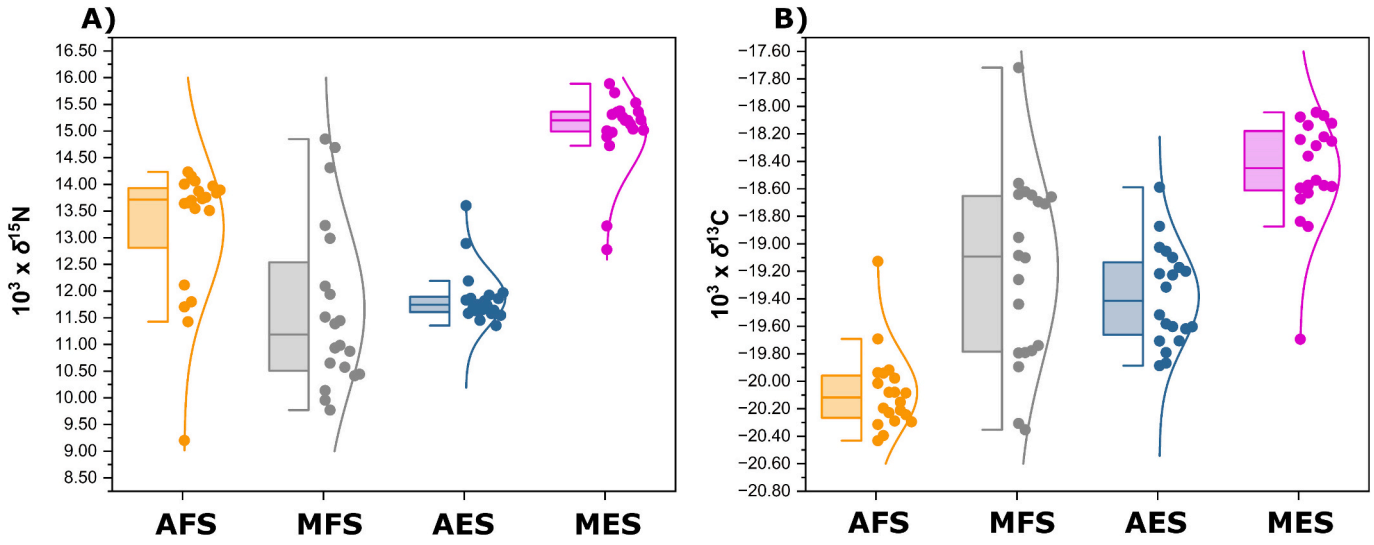

Fig. 2. Box plots with data points and distribution curves of 10^3 x δ^{15}N (**A**) and 10^3 x δ^{13}C (**B**) values measured in Atlantic Flying squids (AFS), Mediterranean flying squids (MFS), Atlantic European squids (AES), and Mediterranean European squids (MES). Boxes: lower 25% quartile, median, and upper 75% quartile; whiskers: 2 times the interquartile range.

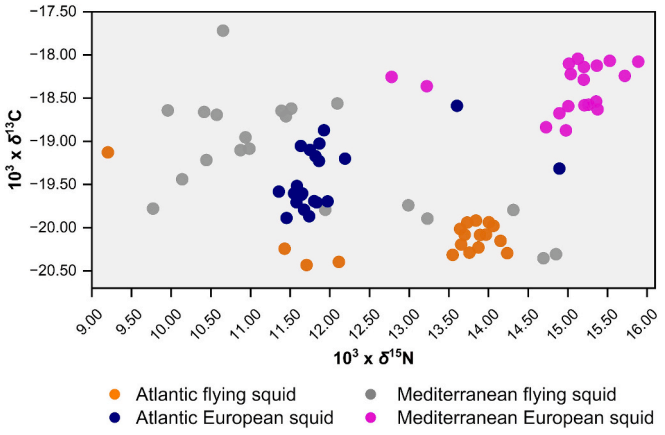

Fig. 3. Two-dimensional score scatter plot showing the distribution of flying squids and European squids from the Atlantic Ocean and the Mediterranean Sea based on 10^3 x δ^{15}N and 10^3 x δ^{13}C values.

Atlantic Ocean (AES vs. AFS). On the contrary, in the Atlantic samples, flying squids generally exhibited lower δ^{13}C values compared to European squid (Fig. 3). In summary, the analysis indicated that relying solely on δ^{13}C and δ^{15}N values may not provide an adequate basis for establishing a distinct separation of samples according to their isotopic signatures.

The *k*-means cluster analysis, conducted by combining both the isotopic and the 13-lanthanide signatures, was designed with the selection of two clusters (*k*), determined after the computation of the Silhouette coefficients. Results from the Silhouette analysis are summarized in Fig. 4. In Fig. 4A, the Silhouette coefficient values obtained by testing 2–15 cluster configurations are reported, while Fig. 4B illustrates the Silhouette plot for the optimal $k = 2$ configuration. As observed, the highest Silhouette coefficients (equal to 0.694) was achieved when the number of clusters was set to 2 (Fig. 4A, Fig. 4B), while a progressive decline in its values was noted at *k* ranging from 3 to 15 (0.689–0.403). The score plot depicting the distribution of samples into the chosen two clusters is presented in Fig. 5. The results revealed the presence of a first, smaller, and more homogeneous cluster (including 25 out of 80 squids) located on the left part of the plot, which encompassed samples all characterized by negative scores on the principal component

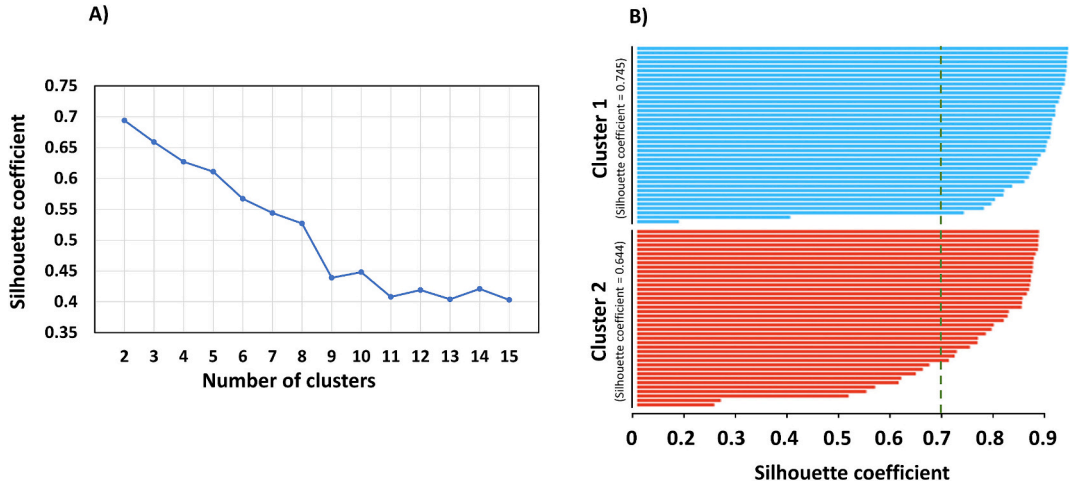

Fig. 4. Results of the Silhouette method for *k*-means cluster analysis showing the Silhouette coefficients for 2 up to 15 clusters (A) and the Silhouette plot for the optimal number ($k = 2$) of clusters (B).

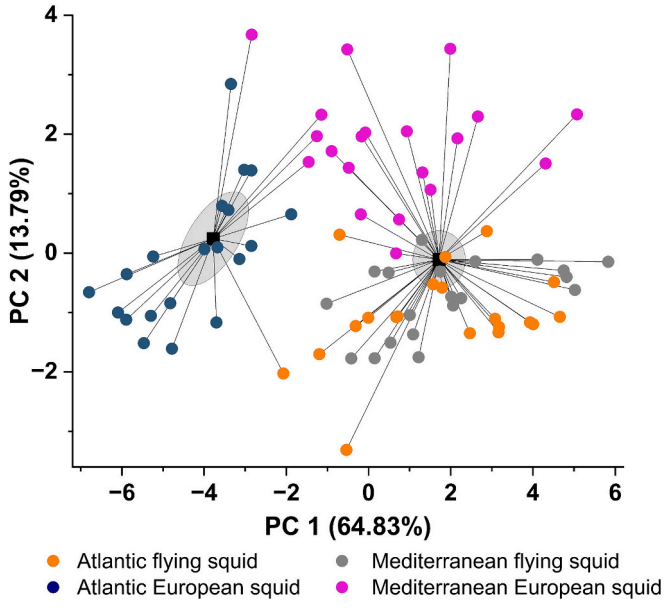

Fig. 5. Score scatter plot resulting from the application of the *k*-means cluster analysis showing the distribution of flying squids and European squids from the Atlantic Ocean and the Mediterranean Sea based on combined isotope ratios and lanthanide concentrations (centroids of each cluster are represented by grey squares).

1 (PC1). Notably, all the 20 AES samples cohesively grouped within this first cluster, although 1 AFS sample and 4 MES samples overlapped within it (Fig. 5). All the 20 AFS and 19 out of 20 MFS samples were identified within the second (right) cluster, together with the majority of MES samples (Fig. 5). Interestingly, MES samples were distributed predominantly at the top of the cluster, showing mostly positive scores on the PC2. In contrast, AFS and MFS samples exhibited overlap at the bottom of the cluster, showing mainly negative scores on the PC2. This outcome suggest that flying squids shared a very similar isotopic and lanthanide composition, posing challenges in their differentiation with respect to their Mediterranean or Atlantic origin using *k*-means clustering.

Despite this evidence, upon analyzing and visually assessing inter-cluster distances, it was found that coupling lanthanide profiles with isotope profiles enhanced the spatial resolution related to the distribution of samples based on their biological species compared to using isotopic ratios alone (Fig. 3). However, *k*-means cluster analysis, as an unsupervised technique, was not decisive for the clear separation of squids into the four groups of interest.

3.3. Classification rules for squid species and geographical origins based on CART analysis

The results obtained through the application of the CART analysis to the training set ($N = 60$) are depicted in Fig. 6. The resulting classification tree displayed a four-level structure, encompassing a total of seven nodes and four decision rules. From the original set of fifteen variables, three were identified as pivotal for partitioning the samples into distinct groups: specifically, the two isotope ratio values of C and N coupled with one lanthanide variable, Pr.

The initial splitting variable was identified as $\delta^{13}C$, with values $\leq -19.91‰$ leading to the classification of 15 out of 15 AFS training samples at tree level one. It is worth noting that 1 MFS sample was erroneously classified within the AFS category, highlighting that classification errors were predominantly associated with the geographical origin of the samples rather than their biological species (Fig. 6).

The optimal classification rules for AES samples were defined by values of $\delta^{13}C > -19.91‰$ in conjunction with Pr concentrations ≤ 0.49 μg kg^{-1}. At level two of the decision tree, this criterion resulted in the accurate classification of 15 out of 15 training samples within the AES class. However, 1 MES sample was incorrectly assigned to the AES class, underscoring once more the greater challenge in correctly identifying sample origin rather than species (Fig. 6).

For MFS samples, the optimal classification rules were determined by $\delta^{13}C > -19.91‰$ in conjunction with Pr concentrations >0.49 μg kg^{-1} and $\delta^{15}N$ values $\leq 14.87‰$. Following these criteria, at level three, 14 out of 15 training samples were accurately classified. On the other hand, the classification of 11 out of 15 training MES samples was achieved by simultaneously considering $\delta^{13}C > -19.91‰$, Pr concentrations >0.49 μg kg^{-1}, and $\delta^{15}N$ values $>14.87‰$ (Fig. 5).

Based on the performance metrics presented in Table 2, the highest values of accuracy, precision, sensitivity, and specificity were observed during the training phase of the CART model, as opposed to its application to the external validation set. Indeed, all the metrics exhibited a modest decline of approximately 5–12% during the validation phase (Table 2), although they can still be deemed satisfactory, since globally higher than 80.0%. More specifically, the highest accuracy values when validating the trained model, reaching 95.0%, were achieved when classifying AES and MES samples. The classification of AES test samples also yielded the highest sensitivity values, with a perfect score of 100%, denoting the remarkable capability of the model to correctly identify true positive samples belonging to this group. Conversely, the lowest sensitivity values (60.0%) were observed following the classification of AFS test samples (Table 2). In general, the classification of MFS samples resulted in the least favorable metrics. This was primarily attributed to the presence of both false positive ($N = 2$) and false negative ($N = 1$) samples in the misclassification matrix, which introduced confusion in the accurate assignment of samples to their appropriate classes (Table 2).

The above results were further confirmed by evaluating the ROC curves reported in Fig. 7 and comparing the AUROC values for each of the squid groups under investigation. The highest AUROC values in both the training and test sets were achieved for AES samples, with AUROC scores of 0.989 and 0.967, respectively. In contrast, the lowest AUROC values were observed for MES samples in the training sets (AUROC = 0.937), and for AFS samples in the test set (AUROC = 0.767). These AUROC values, all exceeding the threshold of 0.500, confirm the discriminatory power of the model and provide evidence that its performances are not merely a result of randomness.

4. Discussion

The $\delta^{13}C$ and $\delta^{15}N$ reflection of trophic dynamics, feeding habits, and prey availability within the aquatic environment has been exploited in the present study to discriminate between two economically important squid species sourced from the North-Eastern Atlantic Ocean and the Northern Adriatic Sea (Central Mediterranean). Seawaters near to polar latitudes, characterized by lower temperatures, were reported to show greater negative $\delta^{13}C$ values, reflecting a diminished $^{13}C/^{12}C$ ratio (i.e., a greater depletion of the ^{13}C isotope) (Carrera & Gallardo, 2017; Kim et al., 2015). This phenomenon was confirmed by the results achieved, albeit observed on a localized scale. Indeed, the analyzed flying squids and European squids from the Atlantic Ocean, inhabiting regions in closer proximity to the poles, displayed more negative $\delta^{13}C$ values when compared to their counterparts collected from the Mediterranean Sea, situated nearer to the equator, and characterized by higher sea surface temperatures (Table 1). On the other side, $\delta^{13}C$ variations were also attributed to the feeding behaviors typical of the species, where higher $\delta^{13}C$ values (more enriched in ^{13}C isotope) were reported for marine species consuming benthic prey (Tanaka et al., 2010). Even though flying squids are bentho-pelagic species (whose prey also includes a significant proportion of organisms living near the seafloor, such as bivalve mollusks, crustaceans, and worms), while European squids are

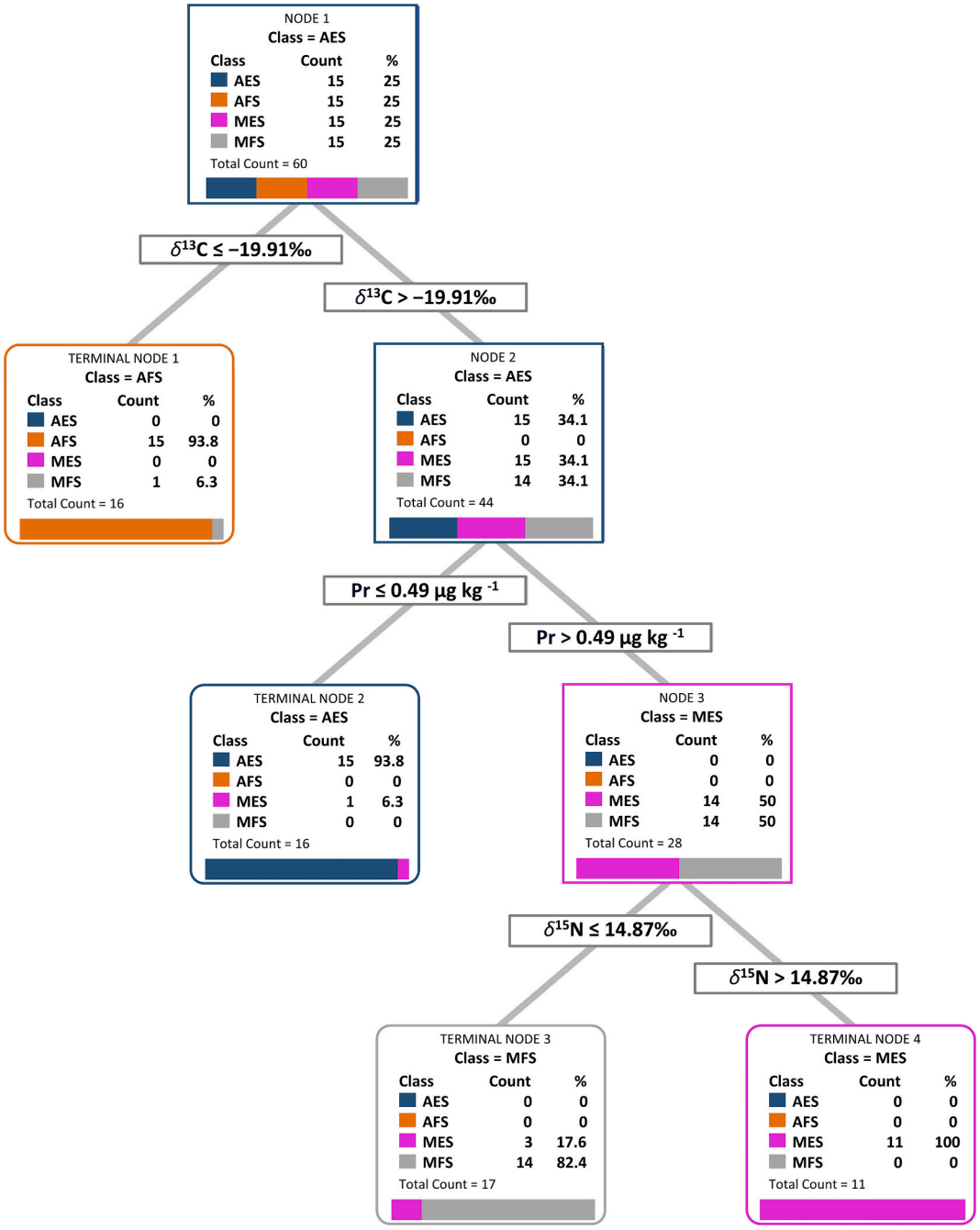

Fig. 6. Classification tree from CART analysis based on isotope ratios and lanthanide concentrations showing decisions rules for the classification of Atlantic flying squids (AFS), Mediterranean flying squids (MFS), Atlantic European squids (AES), and Mediterranean European squids (MES). Within each node: count = number of samples classified in each class; % = percentage precision values of classification.

mainly neritic species (whose prey is often suspended in the water, such as smaller fish) (Chouvelon et al., 2011), an opposite trend was observed in the present work. Indeed, with equal geographical provenance, the bentho-pelagic flying squids showed lower (rather than higher) $\delta^{13}C$ values compared to the neritic European squids (Table 1), leading ambiguous or uncertain interpretations regarding the possibility of using $\delta^{13}C$ as a univocal marker of species.

Deciphering the significance of the N isotopic signature observed in the analyzed squid samples was also found to be very challenging due to the complexity of the results obtained. Species-related differences in terms of $\delta^{15}N$ values among flying squids and European squids were not clearly observed, probably due to the small differences of feeding behavior between European and flying squids. Indeed, concerning the Atlantic samples, an enrichment in the ^{15}N isotope was observed in flying squids compared to European squids. Conversely, in the case of Mediterranean samples, European squids exhibited the highest enrichment in ^{15}N (Table 1, Fig. 2, Fig. 3).

In contrast to several studies where the use of $\delta^{13}C$ and $\delta^{15}N$ alone was sufficient for discriminating different type of fishery products (fish, mollusks, and crustaceans) by both geographical origin and species with a high degree of accuracy (Bianchini et al., 2021; Carrera & Gallardo, 2017; Li et al., 2018; Monteiro Oliveira et al., 2011), the outcomes of the present study diverged from these findings. Conversely, they are in line with other studies which have found it necessary to combine additional data from chemical markers beyond isotope ratios, such as multi-elemental and fatty acid compositions, to achieve satisfactory

Table 2
Misclassification matrices and performance metrics of the CART model classifying Atlantic European squid (AES), Atlantic flying squid (AFS), Mediterranean European squid (MES), and Mediterranean flying squid (MFS) samples during calibration with the training set ($N = 60$) and validation with the test set ($N = 20$).

	Predicted Class (Training set)								
Actual Class	Tot N.	AES	AFS	MES	MFS	Accuracy (%)	Precision (%)	Sensitivity (%)	Specificity (%)
AES	15	15	0	0	0	98.3	93.8	100	97.8
AFS	15	0	15	0	0	98.3	93.8	100	97.8
MES	15	1	0	11	3	93.3	100	73.3	100
MFS	15	0	1	0	14	93.3	82.4	93.3	93.3
All	60	16	16	11	17	95.8	92.5	91.7	97.2
	Predicted Class (Test set)								
Actual Class	Tot. N	AES	AFS	MES	MFS	Accuracy (%)	Precision (%)	Sensitivity (%)	Specificity (%)
AES	5	5	0	0	0	95.0	83.3	100	93.3
AFS	5	0	3	0	2	85.0	75.0	60.0	93.3
MES	5	1	0	4	0	95.0	100	80.0	100.0
MFS	5	0	1	0	4	85.0	66.7	80.0	86.7
All	20	6	4	4	6	90.0	81.3	80.0	93.3

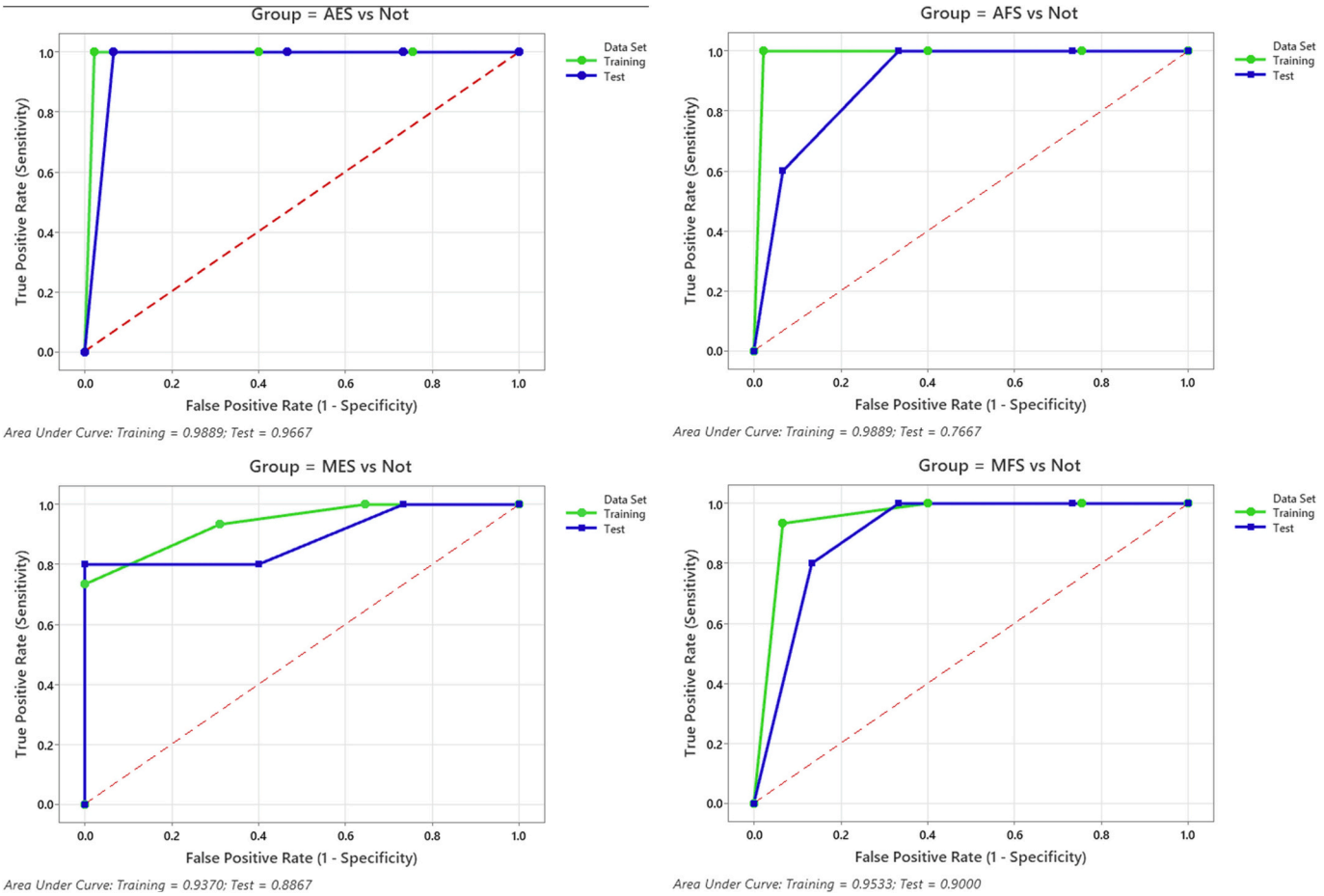

Fig. 7. Area Under the Receiver Operating Characteristic (AUROC) curves for Atlantic European squid (AES), Atlantic flying squid (AFS), Mediterranean European squid (MES), and Mediterranean flying squid (MFS) samples during calibration with the training set (N = 60) and validation with the test set (N = 20).

classification results (Carter et al., 2015; Gong et al., 2018; Luo et al., 2019; Martino et al., 2022; Ni et al., 2022; Vasconi et al., 2019).

When considering each squid species separately, higher concentrations of lanthanides were found in Mediterranean samples compared to those from the Atlantic Ocean (Table 1). This result could be attributed to typically lower lanthanide concentrations reported in open ocean regions, contrasting with higher levels found in coastal areas where continuous anthropogenic inputs are more prevalent (Piarulli et al., 2021). Studies indicate that Mediterranean surface waters exhibit significant lanthanide enrichment compared to nearby Atlantic waters, suggesting ongoing lanthanide inputs along the circulation in this specific region (Garcia-Solsona & Jeandel, 2020). On the other hand, marine organisms that feed on sediments are known to be more prone to lanthanide uptake (Mayfield & Fairbrother, 2015; Piarulli et al., 2021) and this phenomenon may account for the higher concentrations observed in the bentho-pelagic flying squids compared to their neritic European squids, as outlined in Table 1.

As shown in the score plot depicted in Fig. 4, the application of *k*-

means cluster analysis revealed an enhancement in the categorization of squid samples when stable isotope ratios were integrated with lanthanide profiles. This outcome validates the potential of lanthanides to provide an additional informational dimension for the authentication of squid, ultimately leading to more robust conclusions regarding their origins and species. This effect was found to be more pronounced in the case of European squids which, globally, exhibited a trend in separating not only from flying squids but also among themselves based on their Atlantic or Mediterranean origin. Conversely, flying squids from the two distinct sampling regions displayed a considerable degree of overlap, implying that the information pertaining to their provenance and encapsulated within the lanthanide profile was comparatively less discriminatory for this biological species.

The significant variation in lanthanide concentrations among the four squid groups (Table 1) resulted in quite consistent patterns of both positive and negative bivariate correlations across the various groups, albeit varying degrees of strength of these correlations were found (Fig. 1). This observation indicates that the distribution of all the lanthanides was quite consistent and uniform across all the analyzed specimens. This consistency can be attributed to the shared chemical and physical properties of these elements, which allowed them to be assimilated into squid tissues through similar pathways. This trend is not novel and has previously been documented in other food products, including milk and cuttlefish (Aceto et al., 2017; Varrà et al., 2021).

From the authors' viewpoint, the above findings bear a positive implication as they indicate the presence of redundant information conveyed by multiple lanthanide markers, opening the possibility of streamlining the analysis by focusing solely on the most significant variables. The potential to eliminate the need for measuring and quantifying the entire range of lanthanides was indeed confirmed through the construction of a simple and highly interpretable decision tree based on CART analysis. The decision rules generated by applying the CART algorithm were indeed very parsimonious, incorporating only 3 out of the original 15 variables, which consisted of a combination of both stable isotope ratios and one lanthanide element, as illustrated in Fig. 6. The determined threshold values for $\delta^{13}C$, $\delta^{15}N$, and Pr collectively formed an effective decision-making process that demonstrated remarkable performance metrics also when discerning the class membership of unknown squid specimens included in the test set (Table 2), thus increasing the confidence in the utility of this tool for practical applications.

It is worth noting that while these metrics—expressed in terms of accuracy, precision, sensitivity, and specificity—were impressive, they did not reach 100%. This outcome can be attributed not only to the relatively limited sample size but also to the high inherent biological variability of the squid samples and the complex relationships between the isotopes and lanthanides used as chemical markers. Furthermore, while 100% classification performance could potentially be achieved by increasing the complexity and depth of the CART model, this would risk overfitting, capturing noise rather than true underlying patterns.

Overall, it is important to acknowledge that the use of decision trees as a machine learning technique for food authentication and traceability still remains relatively uncommon, with only a few prior studies focusing on plant-based foods and rarely measuring lanthanides (Maione et al., 2016; Sim et al., 2023; Vanderschueren et al., 2019). Consequently, making direct comparisons and drawing conclusions from the results in the context of existing literature poses significant challenges. Furthermore, offering a biological and ecological significance for Pr, as well as an explanation for its superior predictive capabilities compared to other lanthanides in distinguishing squid samples by species and origin, becomes even more intricate due to the absence of prior research dedicated to this specific element. However, there is evidence to support the idea that Pr can persist in fish tissue for a long time, which strongly suggests its potential use as a marker for various authenticity attributes in fishery products (Pérez de Nanclares et al., 2016; Wang et al., 2019).

In conclusions, the results presented in this work validate the initial hypothesis that the integration of complementary information derived from $\delta^{13}C$, $\delta^{15}N$, and lanthanides is an effective and straightforward approach for the simultaneous recognition of the geographical origin and biological species of squids. However, the findings achieved have also raised significant, unresolved questions, necessitating further research studies aimed at clarifying the role of lanthanides and their interaction with stable isotopes of light elements in aquatic environments, as well as at confirming their utility as synergistic markers for assuring seafood authenticity and traceability across a broader spectrum of provenances and species.

5. Conclusions

The present study employed CART analysis to construct a decision tree, revealing that the key variables for sample classification of squids based on both their origin (North-Eastern Atlantic Ocean and Central Mediterranean Sea) and species (European squid-*Loligo vulgaris* and flying squid-*Todarodes sagittatus*) were $\delta^{13}C$ and $\delta^{15}N$ values in conjunction with Pr concentrations. Using just these three parameters and establishing specific threshold values to create classification rules, an average accuracy of 90% in sample recognition was achieved. Hence, reducing the analysis to only three essential variables can be effective, particularly for preliminary screening, in identifying the authenticity of cephalopods regarding their origin and species and thus identify potential fraud with important economic and safety implications.

While this approach may appear somewhat contrary to the prevailing trend of contemporary research of generating and integrating extensive data from multiple analytical platforms, it underscores the practical value of streamlined methodologies in addressing the unique complexities of the fish supply network. The high level of interpretability, ease of deployment, cost-efficiency, and versatility of this tool make it well-suited to meet the needs of food business operators at all levels of the seafood industry. It is not only applicable within the framework of own-check systems but also aligns with the requirements of competent authorities involved in official controls and inspection procedures. The implementation of this approach would, therefore, significantly enhance traceability systems for fishery products, ultimately strengthening the promotion of transparency and the mitigation of food safety hazards within fishery sector.

Funding

This work was supported by the University of Pardubice, Grant Number SGS_2024_001.

CRediT authorship contribution statement

Maria Olga Varrà: Writing – original draft, Software, Investigation, Data curation. **Lenka Husáková:** Writing – review & editing, Supervision, Methodology, Funding acquisition. **Paola Iacumin:** Writing – review & editing, Validation, Methodology. **Martina Piroutková:** Formal analysis. **Mattia Rossi:** Formal analysis. **Jan Patočka:** Formal analysis. **Sergio Ghidini:** Writing – review & editing, Conceptualization. **Emanuela Zanardi:** Writing – review & editing, Supervision, Project administration, Conceptualization.

Declaration of competing interest

The authors declare that they have no known competing financial interests or personal relationships that could have appeared to influence the work reported in this paper.

Data availability

The dataset generated during the current study will be made

available on reasonable request.

Appendix A. Supplementary data

Supplementary data to this article can be found online at https://doi.org/10.1016/j.foodchem.2024.140303.

References

Aceto, M., Musso, D., Calà, E., Arieri, F., & Oddone, M. (2017). Role of lanthanides in the traceability of the Milk production chain. *Journal of Agricultural and Food Chemistry, 65*(20), 4200–4208. https://doi.org/10.1021/acs.jafc.7b00916

Bianchini, G., Brombin, V., Carlino, P., Mistri, E., Natali, C., & Salani, G. M. (2021). Traceability and authentication of Manila clams from North-Western Adriatic lagoons using C and N stable isotope analysis. *Molecules, 26*(7). https://doi.org/10.3390/molecules26071859. Article 7.

Carrera, M., & Gallardo, J. M. (2017). Determination of the geographical origin of all commercial hake species by stable isotope ratio (SIR) analysis. *Journal of Agricultural and Food Chemistry, 65*(5), 1070–1077. https://doi.org/10.1021/acs.jafc.6b04972

Carter, J. F., Tinggi, U., Yang, X., & Fry, B. (2015). Stable isotope and trace metal compositions of Australian prawns as a guide to authenticity and wholesomeness. *Food Chemistry, 170*, 241–248. https://doi.org/10.1016/j.foodchem.2014.08.037

Chouvelon, T., Spitz, J., Cherel, Y., Caurant, F., Sirmel, R., Mèndez-Fernandez, P., & Bustamante, P. (2011). Inter-specific and ontogenic differences in δ13C and δ15N values and hg and cd concentrations in cephalopods. *Marine Ecology Progress Series, 433*, 107–120. https://doi.org/10.3354/meps09159

Costa Leal, M., Pimentel, T., Ricardo, F., Rosa, R., & Calado, R. (2015). Seafood traceability: Current needs, available tools, and biotechnological challenges for origin certification. *Trends in Biotechnology, 33*(6), 331–336. https://doi.org/10.1016/j.tibtech.2015.03.003

Danezis, G. P., Pappas, A. C., Zoidis, E., Papadomichelakis, G., Hadjigeorgiou, I., Zhang, P., … Georgiou, C. A. (2017). Game meat authentication through rare earth elements fingerprinting. *Analytica Chimica Acta, 991*, 46–57. https://doi.org/10.1016/j.aca.2017.09.013

Danezis, G. P., Tsagkaris, A. S., Brusic, V., & Georgiou, C. A. (2016). Food authentication: State of the art and prospects. *Current Opinion in Food Science, 10*, 22–31. https://doi.org/10.1016/j.cofs.2016.07.003

Danezis, G. P., Tsagkaris, A. S., Camin, F., Brusic, V., & Georgiou, C. A. (2016). Food authentication: Techniques, trends & emerging approaches. *TrAC Trends in Analytical Chemistry, 85*, 123–132. https://doi.org/10.1016/j.trac.2016.02.026

European Commission. (2002). Regulation (EC) No 178/2002 of the European Parliament and of the Council of 28 January 2002 laying down the general principles and requirements of food law, establishing the European Food Safety Authority and laying down procedures in matters of food safety. http://data.europa.eu/eli/reg/2002/178/oj/eng.

European Union. (2013). Regulation (EU) No 1379/2013 of the European Parliament and of the Council of 11 December 2013 on the common organisation of the markets in fishery and aquaculture products, amending Council Regulations (EC) No 1184/2006 and (EC) No 1224/2009 and repealing Council Regulation (EC) No 104/2000. http://data.europa.eu/eli/reg/2013/1379/oj/eng.

Fawcett, T. (2006). An introduction to ROC analysis. *Pattern Recognition Letters, 27*(8), 861–874. https://doi.org/10.1016/j.patrec.2005.10.010

Garcia-Solsona, E., & Jeandel, C. (2020). Balancing rare earth element distributions in the northwestern Mediterranean Sea. *Chemical Geology, 532*, Article 119372. https://doi.org/10.1016/j.chemgeo.2019.119372

Gong, Y., Li, Y., Chen, X., & Chen, L. (2018). Potential use of stable isotope and fatty acid analyses for traceability of geographic origins of jumbo squid (*Dosidicus gigas*). *Rapid Communications in Mass Spectrometry, 32*(7), 583–589. https://doi.org/10.1002/rcm.8071

Guardone, L., Tinacci, L., Costanzo, F., Azzarelli, D., D'Amico, P., Tasselli, G., Magni, A., Guidi, A., Nucera, D., & Armani, A. (2017). DNA barcoding as a tool for detecting mislabeling of fishery products imported from third countries: An official survey conducted at the border inspection post of Livorno-Pisa (Italy). *Food Control, 80*, 204–216. https://doi.org/10.1016/j.foodcont.2017.03.056

Jiménez-Carvelo, A. M., González-Casado, A., Bagur-González, M. G., & Cuadros-Rodríguez, L. (2019). Alternative data mining/machine learning methods for the analytical evaluation of food quality and authenticity – A review. *Food Research International, 122*, 25–39. https://doi.org/10.1016/j.foodres.2019.03.063

Katerinopoulou, K., Kontogeorgos, A., Salmas, C. E., Patakas, A., & Ladavos, A. (2020). Geographical origin authentication of Agri-food products: A review. *Foods, 9*(4), Article 4. https://doi.org/10.3390/foods9040489

Khaksar, R., Carlson, T., Schaffner, D. W., Ghorashi, M., Best, D., Jandhyala, S., … Amini, S. (2015). Unmasking seafood mislabeling in U.S. markets: DNA barcoding as a unique technology for food authentication and quality control. *Food Control, 56*, 71–76. https://doi.org/10.1016/j.foodcont.2015.03.007

Kim, H., Suresh Kumar, K., & Shin, K.-H. (2015). Applicability of stable C and N isotope analysis in inferring the geographical origin and authentication of commercial fish (mackerel, yellow croaker and Pollock). *Food Chemistry, 172*, 523–527. https://doi.org/10.1016/j.foodchem.2014.09.058

Li, L., Ren, W., Dong, S., & Feng, J. (2018). Investigation of geographic origin, salinity and feed on stable isotope profile of Pacific white shrimp (*Litopenaeus vannamei*). *Aquaculture Research, 49*(2), 1029–1036. https://doi.org/10.1111/are.13551

Luo, R., Jiang, T., Chen, X., Zheng, C., Liu, H., & Yang, J. (2019). Determination of geographic origin of Chinese mitten crab (*Eriocheir sinensis*) using integrated stable isotope and multi-element analyses. *Food Chemistry, 274*, 1–7. https://doi.org/10.1016/j.foodchem.2018.08.104

Maione, C., Batista, B. L., Campiglia, A. D., Barbosa, F., & Barbosa, R. M. (2016). Classification of geographic origin of rice by data mining and inductively coupled plasma mass spectrometry. *Computers and Electronics in Agriculture, 121*, 101–107. https://doi.org/10.1016/j.compag.2015.11.009

Martino, J. C., Doubleday, Z. A., & Gillanders, B. M. (2019). Metabolic effects on carbon isotope biomarkers in fish. *Ecological Indicators, 97*, 10–16. https://doi.org/10.1016/j.ecolind.2018.10.010

Martino, J. C., Mazumder, D., Gadd, P., & Doubleday, Z. A. (2022). Tracking the provenance of octopus using isotopic and multi-elemental analysis. *Food Chemistry, 371*, Article 131133. https://doi.org/10.1016/j.foodchem.2021.131133

Mayfield, D. B., & Fairbrother, A. (2015). Examination of rare earth element concentration patterns in freshwater fish tissues. *Chemosphere, 120*, 68–74. https://doi.org/10.1016/j.chemosphere.2014.06.010

Miedico, O., Iammarino, M., Pompa, C., Tarallo, M., & Chiaravalle, A. E. (2015). Assessment of lead, cadmium and mercury in seafood marketed in Puglia and Basilicata (Italy) by inductively coupled plasma mass spectrometry. *Food Additives & Contaminants: Part B, 8*(2), 85–92. https://doi.org/10.1080/19393210.2014.989281

Monteiro Oliveira, E. J. V., Sant'Ana, L. S., Ducatti, C., Denadai, J. C., & de Souza Kruliski, C. R. (2011). The use of stable isotopes for authentication of gadoid fish species. *European Food Research and Technology, 232*(1), 97–101. https://doi.org/10.1007/s00217-010-1367-7

Ni, X., Li, X., Ran, G., Chen, J., Jiang, X., Sun, J., & Bai, W. (2022). Determination of the geographical origin of *Trachinotus ovatus* and *Pampus argenteus* in China by multi-element and stable isotope analysis. *Food Chemistry, 394*, Article 133457. https://doi.org/10.1016/j.foodchem.2022.133457

Patel, K. S., Sharma, S., Maity, J. P., Martín-Ramos, P., Fiket, Ž., Bhattacharya, P., & Zhu, Y. (2023). Occurrence of uranium, thorium and rare earth elements in the environment: A review. *Frontiers in environmental Science, 10*. https://www.frontiersin.org/articles/10.3389/fenvs.2022.1058053.

Pérez de Nanclares, M., Dessen, J.-E., Rørvik, K.-A., Thomassen, Y., & Thomassen, M. S. (2016). Feasibility of using rare earth elements (REEs) to mark and identify escaped farmed Atlantic salmon *Salmo salar* L. *Aquaculture Research, 47*(6), 1885–1898. https://doi.org/10.1111/are.12647

Piarulli, S., Hansen, B. H., Ciesielski, T., Zocher, A.-L., Malzahn, A., Olsvik, P. A., … Farkas, J. (2021). Sources, distribution and effects of rare earth elements in the marine environment: Current knowledge and research gaps. *Environmental Pollution, 291*, Article 118230. https://doi.org/10.1016/j.envpol.2021.118230

del Rio-Lavín, A., Weber, J., Molkentin, J., Jiménez, E., Artetxe-Arrate, I., & Pardo, M.Á. (2022). Stable isotope and trace element analysis for tracing the geographical origin of the Mediterranean mussel (*Mytilus galloprovincialis*) in food authentication. *Food Control, 139*, Article 109069. https://doi.org/10.1016/j.foodcont.2022.109069

Rosa, R., Pereira, J., & Nunes, M. L. (2005). Biochemical composition of cephalopods with different life strategies, with special reference to a giant squid Architeuthis sp. *Marine Biology, 146*(4), 739–751. https://doi.org/10.1007/s00227-004-1477-5

Rousseeuw, P. J. (1987). Silhouettes: A graphical aid to the interpretation and validation of cluster analysis. *Journal of Computational and Applied Mathematics, 20*, 53–65. https://doi.org/10.1016/0377-0427(87)90125-7

Sim, J., Mcgoverin, C., Oey, I., Frew, R., & Kebede, B. (2023). Stable isotope and trace element analyses with non-linear machine-learning data analysis improved coffee origin classification and marker selection. *Journal of the Science of Food and Agriculture, 103*(9), 4704–4718. https://doi.org/10.1002/jsfa.12546

Tanaka, H., Ohshimo, S., Takagi, N., & Ichimaru, T. (2010). Investigation of the geographical origin and migration of anchovy *Engraulis japonicus* in Tachibana Bay, Japan: A stable isotope approach. *Fisheries Research, 102*(1), 217–220. https://doi.org/10.1016/j.fishres.2009.11.002

Tulli, F., Moreno-Rojas, J. M., Messina, C. M., Trocino, A., Xiccato, G., Muñoz-Redondo, J. M., … Tibaldi, E. (2020). The use of stable isotope ratio analysis to trace European Sea bass (*D. Labrax*) originating from different farming systems. *Animals, 10*(11). https://doi.org/10.3390/ani10112042. Article 11.

Vanderschueren, R., Montalvo, D., De Ketelaere, B., Delcour, J. A., & Smolders, E. (2019). The elemental composition of chocolates is related to cacao content and origin: A multi-element fingerprinting analysis of single origin chocolates. *Journal of Food Composition and Analysis, 83*, Article 103277. https://doi.org/10.1016/j.jfca.2019.103277

Varrà, M. O., Ghidini, S., Zanardi, E., Badiani, A., & Ianieri, A. (2019). Authentication of European sea bass according to production method and geographical origin by light stable isotope ratio and rare earth elements analyses combined with chemometrics. *Italian. Journal of Food Safety, 8(1), Article 1*. https://doi.org/10.4081/ijfs.2019.7872

Varrà, M. O., Husáková, L., Patočka, J., Ghidini, S., & Zanardi, E. (2021). Multi-element signature of cuttlefish and its potential for the discrimination of different geographical provenances and traceability. *Food Chemistry, 356*, Article 129687. https://doi.org/10.1016/j.foodchem.2021.129687

Varrà, M. O., Husáková, L., Patočka, J., Ianieri, A., Ghidini, S., & Zanardi, E. (2023). Cadmium, lead, and mercury in two commercial squid species from the North Adriatic Sea (Central Mediterranean): Contamination levels and health risk assessment. *Italian Journal of Food Safety, 12*(2), 11037. https://doi.org/10.4081/ijfs.2023.11037

Varrà, M. O., Zanardi, E., Serra, M., Conter, M., Ianieri, A., & Ghidini, S. (2023). Isotope fingerprinting as a backup for modern safety and traceability systems in the animal-derived food chain. *Molecules, 28*(11), 4300. https://doi.org/10.3390/molecules28114300

Vasconi, M., Lopez, A., Galimberti, C., Moreno Rojas, J. M., Muñoz Redondo, J. M., Bellagamba, F., & Moretti, V. M. (2019). Authentication of farmed and wild european eel (*Anguilla anguilla*) by fatty acid profile and carbon and nitrogen isotopic analyses. *Food Control, 102*, 112–121. https://doi.org/10.1016/j.foodcont.2019.03.004

Wang, Z., Yin, L., Xiang, H., Qin, X., & Wang, S. (2019). Accumulation patterns and species-specific characteristics of yttrium and rare earth elements (YREEs) in biological matrices from Maluan Bay, China: Implications for biomonitoring. *Environmental Research, 179*, Article 108804. https://doi.org/10.1016/j.envres.2019.108804

Xu, Y., Peng, K., Jiang, F., Cui, Y., Han, D., Liu, H., Hong, H., & Tian, X. (2022). Geographical discrimination of swimming crabs (*Portunus trituberculatus*) using stable isotope and multi-element analyses. *Journal of Food Composition and Analysis, 105*, Article 104251. https://doi.org/10.1016/j.jfca.2021.104251

Zhang, X., Liu, Y., Li, Y., & Zhao, X. (2017). Identification of the geographical origins of sea cucumber (*Apostichopus japonicus*) in northern China by using stable isotope ratios and fatty acid profiles. *Food Chemistry, 218*, 269–276. https://doi.org/10.1016/j.foodchem.2016.08.083